

Light enhancement by metal-insulator-metal plasmonic focusing cavity

J. Wen^{1,2} · W. J. Wang^{1,3} · N. Li¹ · Z. F. Li¹ ·
W. Lu¹

Received: 29 September 2015 / Accepted: 3 November 2015 / Published online: 29 January 2016
© Springer Science+Business Media New York 2016

Abstract A Metal-Insulator-Metal (MIM) plasmonic focusing cavity intended to be applied on the avalanche photodiode (APD) is simulated. The structure includes a large upper metallic grating to couple incident light into the cavity and a small lower metallic grating to couple the light into the APD below the MIM cavity. The optical properties of the cavity are investigated in detail. Our results provide a possibility to reduce the dark current of an InGaAs/InP APD operated under the Geiger mode by decreasing the photo-sensitive area of the APD, while remaining its high detection efficiency by remaining a large light collection area.

Keywords Avalanche photodiode · Light enhancement · Focusing · Cavity · Finite difference time domain simulation

1 Introduction

Geiger-mode avalanche photodiode (APD) is widely used in single photon detection, especially Si APDs in the visible range (Eisaman et al. 2011). Development of quantum communication requires single photon detection technology with higher detection

This article is part of the Topical Collection on Numerical Simulation of Optoelectronic Devices, NUSOD' 15, Guest edited by Julien Javaloyes, Weida Hu, Slawek Sujecki and Yuh-Renn Wu.

✉ W. J. Wang
wangwj@mail.sitp.ac.cn

¹ National Laboratory of Infrared Physics, Shanghai Institute of Technical Physics, Chinese Academy of Sciences, Shanghai 200083, China

² University of Chinese Academy of Sciences, Beijing 100000, China

³ Synergetic Innovation Center of Quantum Information and Quantum Physics, University of Science and Technology of China, Hefei 230026, Anhui, China

efficiency and lower dark count rate. Because the near infrared wavelength of 1.55 μm is widely used in optical fiber communication, single photon detectors aimed at this band attract more attention. For 1.55 μm , InGaAs/InP APDs are the best choice due to the simplicity and stability of fabrication and a moderate working temperature (Jiang et al. 2007; Beveratos et al. 2002), compared to typical InSb infrared APDs (Abautret et al. 2013), HgCdTe infrared photodetectors (Qiu and Hu 2015; Gopal et al. 2014), and HgCdTe infrared APD (Qiu et al. 2015). However, owing to materials defects, InGaAs/InP APDs suffer from dark count rates that are orders of magnitude higher than for their Si counterparts (Hadfield 2009). An effective method is to reduce the photo-sensitive area, but the quantum efficiency is sacrificed. So, it is crucial for Geiger-mode InGaAs/InP APD to reduce the dark current while keeping the high quantum efficiency.

In this paper, a Metal-Insulator-Metal (MIM) plasmonic focusing cavity is designed to be integrated on our InGaAs/InP APD. The cavity can converge light of specific wavelength to enhance its transmission. Through the MIM cavity, light from a large incident area is efficiently coupled to a small output area. The output light is confined and propagates straight to the APD under the cavity with little divergence. This reduces the photo-sensitive area of the APD with a light collecting area as large as the traditional one, which decreases the dark current efficiently without losing the quantum efficiency.

2 Numerical method and working mechanism

The optical properties of the metal-insulator-metal (MIM) plasmonic focusing cavity we designed are obtained from Maxwell's Equations using finite difference time domain (FDTD) method (Sullivan 2000; Gedney 2011). All of our simulation results are obtained using FDTD Solutions developed by Lumerical Solutions Inc.

FDTD method is a time-stepping method based on the relationship of electric field and magnetic field across space. It discretizes the Maxwell's equations into a series of differential equations using Yee cell. Electromagnetic field is decomposed into six components, E_x , E_y , E_z , H_x , H_y , H_z . If we assume infinity in z direction and make the simulation into a 2-dimensional one, the Maxwell's equations are simplified as follows:

$$\begin{aligned}\varepsilon \frac{\partial E_x}{\partial t} &= \frac{\partial H_z}{\partial y} \\ \varepsilon \frac{\partial E_y}{\partial t} &= \frac{\partial H_z}{\partial x} \\ \frac{\partial H_z}{\partial t} &= -\frac{1}{\mu} \left(\frac{\partial E_y}{\partial x} - \frac{\partial E_x}{\partial y} \right)\end{aligned}\quad (1)$$

The simplified Equations leave us with only three components of the electromagnetic field. If the time step is set as Δt and electric field of t_0 is known to us, then magnetic field of $(t_0 + \Delta t/2)$ and electric field of $(t_0 + \Delta t)$ are obtained sequentially. This process continues iteratively until terminate conditions are reached. Continuous monitoring of residual energy within the simulation region is a way to determine whether the simulation has achieved convergence. Only simulations completed with residual energy low enough are considered valid. The FDTD calculation can provide a view of the light propagation process directly and a transmission spectrum as a function of wavelength after applying Fourier transformation.

In our simulation, the structure is confined in a specific area, thus boundaries of perfectly matched layer are chosen as absorption for the truncation of open-region problem (Rylander and Jin 2004). In this paper, 2D simulation is used to save time and computing memory.

Surface plasmon polariton (SPP) mode plays an important role in our MIM plasmonic focusing cavity. It is one kind of surface plasmon resonance and another resonance mode is localized surface plasmon (LSP). The main property difference of the two resonance modes is whether the resonance is confined within a certain area (Stegeman et al. 1983). LSP is the resonance mode restricted to individual metal structure with no consideration of interaction between different metal structures, thus this resonance mode is strongly dependent on the size and profile of the metal structure (Law et al. 2013). SPP is the electrons resonance with electromagnetic waves coupled to the interface of metal and dielectric. This means that SPP needs to be excited with the wave vector provided by the periodic metal structures. Our cavity works with light converging to the center, so the effective use of SPP mode is the key point of the design.

3 Results and discussions

Figure 1a shows the schematic diagram of the MIM plasmonic focusing cavity. Figure 1b depicts the cross section of the simulated structure.

The material under the MIM cavity is InP, of which the APD is manufactured. The MIM cavity consists of three layers: an upper metallic grating layer, the SiO₂ insulator layer and a lower metallic layer. The lateral boundaries of the cavity are blocked by Au plate. The upper metallic grating is composed of periodic Au bars, and the lower Metallic grating is composed of a center Au bar and two Au plate on its two sides, forming two output holes. The thickness of Au (T_{GRT}) is 0.1 μm and the thickness of the mid SiO₂ (T_{SiO_2}) is 0.3 μm . p is the period of the upper metallic grating and d/p is the duty cycle. For the wavelength of 1.55 μm , the optimized grating parameters are $p = 1.12 \mu\text{m}$ and $d = 0.7 \mu\text{m}$.

The output width of the optical cavity (denoted as S_{out} in Fig. 2) must match with the effective photo-sensitive diameter of the APD, which is shown as the light colored region in InP material. This ensures that light through S_{out} can be absorbed effectively by the

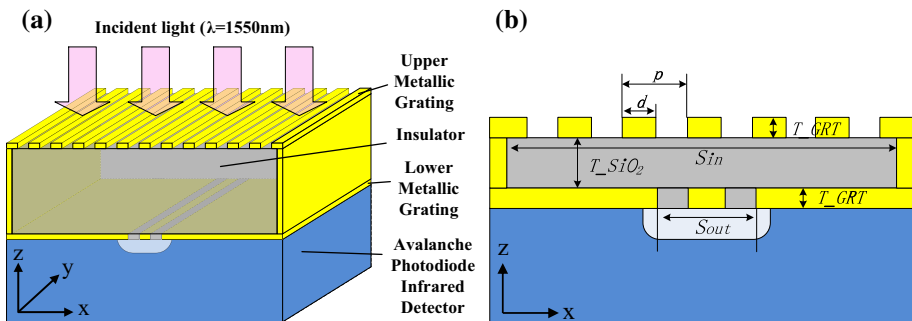
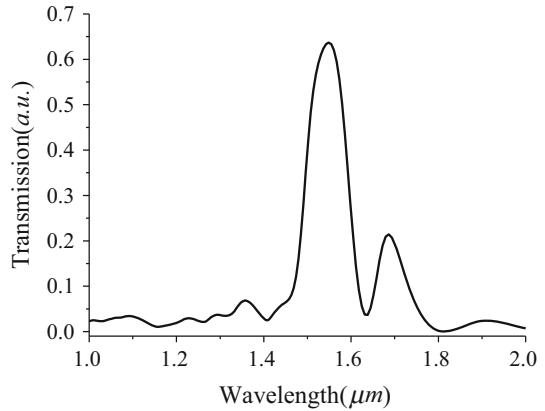


Fig. 1 Simulated structure. **a** Schematic diagram of MIM cavity. **b** Cross section of MIM cavity

Fig. 2 Transmission spectrum of MIM cavity



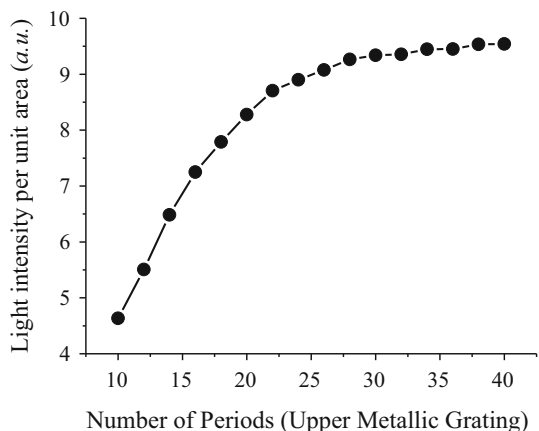
absorption layer of the APD and the volume of the APD can be reduced to 1–2 orders of magnitude, thus the effect of materials defects to the performance can be suppressed.

The transmission spectrum of MIM cavity is shown in Fig. 2. The peak transmission located at 1.55 μm reaches 63.7 %. We consider EF as the light enhancement factor, as shown in Eq. (2). T is the transmission of the MIM cavity.

$$EF = \frac{\frac{P_{out}}{S_{out}}}{\frac{P_{in}}{S_{in}}} = \frac{P_{out}}{P_{in}} \cdot \frac{S_{in}}{S_{out}} = T \cdot \frac{S_{in}}{S_{out}} \tag{2}$$

Figure 3 shows the relationship of the light enhancement factor EF versus the number of periods of the upper metallic grating. If the incident light power per unit area is set as 1, EF represents the output light power per unit area. Since the output width of the optical cavity (S_{out}) is fixed, the bigger EF is, the more output power there is. We can see that when the number of the periods increases, EF is getting bigger and comes to a saturation of 9.3 at about 30 periods. It is difficult for the energy far away from the center to be transmitted to the output hole. The light collection area of the cavity, which is expected to be as large as possible, is decided by the period number. So, the period number of the upper

Fig. 3 Light intensity per unit area varying with the number of periods in the upper metallic grating



grating is set as 30 and the whole incident width is $33.6 \mu\text{m}$, which is similar to the diameter of the traditional APD.

Figure 4 shows the electric field distribution through the MIM cavity. TE light is vertically incident to the MIM cavity. The cavity is located between 0 and $0.5 \mu\text{m}$ in the z direction. As shown in Fig. 4a, $|E_z|^2$ distribution at $1.55 \mu\text{m}$ has a high intensity within the cavity. Since there is no E_z component in the incident light, light resonance is turned into TM mode inside the cavity after passing through the upper metallic grating. Light captured inside the cavity finds its way out through the two holes on the lower metallic grating as TE mode and keep certain intensity during its propagation, as shown in Fig. 4b. From Fig. 4b, we can see that the output light from the lower metallic grating goes straight along the z direction in a confined angle and propagates $2 \mu\text{m}$ with only a divergence angle of $\pm 0.3^\circ$. Because the absorption layer of APD is several micrometers below the surface, this propagation property ensures that the enhanced light can reach the absorption layer of the APD.

Figure 5 shows the transmission spectrum with p varying from 1.02 to $1.22 \mu\text{m}$. Figure 6 shows the transmission spectrum with d varying from 0.64 to $0.76 \mu\text{m}$. When d is fixed as $0.7 \mu\text{m}$, the *PEAK* denoted in Fig. 5 moves from 1.447 to $1.638 \mu\text{m}$ with p increasing from 1.02 to $1.22 \mu\text{m}$, resulting in a red shift of $0.191 \mu\text{m}$. However, when p is fixed as $1.12 \mu\text{m}$, the peak denoted in Fig. 6 moves from 1.525 to $1.561 \mu\text{m}$ with d increasing from 0.64 to $0.76 \mu\text{m}$, resulting in a red shift of $0.036 \mu\text{m}$. Since the variation

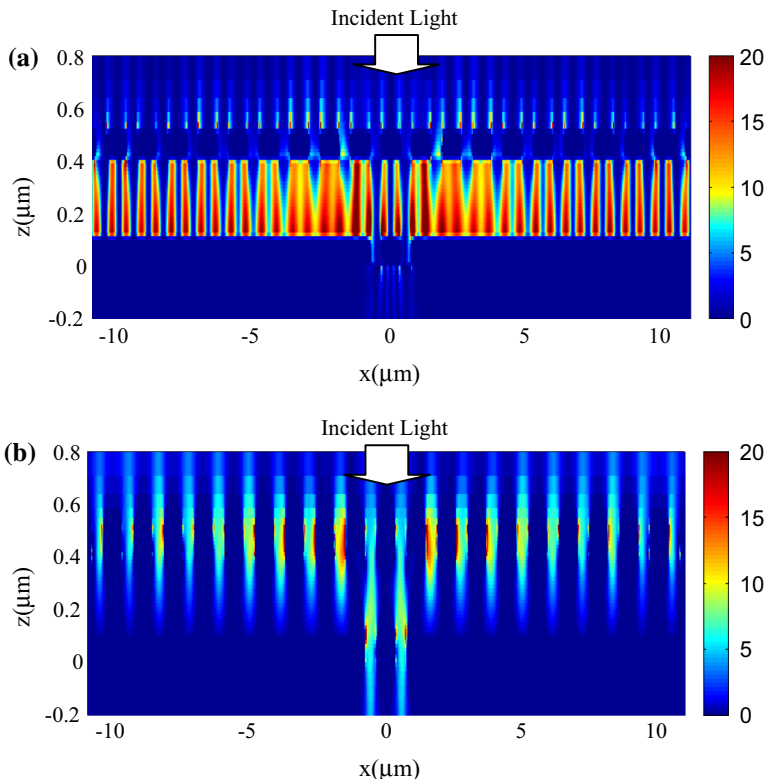


Fig. 4 Electric field distribution at $1.55 \mu\text{m}$. **a** $|E_z|^2$ distribution at $1.55 \mu\text{m}$. **b** $|E_x|^2$ distribution at $1.55 \mu\text{m}$

Fig. 5 Transmission spectrum with p from 1.02 to 1.22 μm

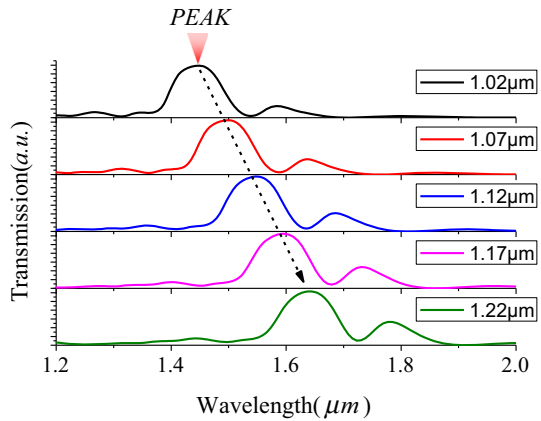
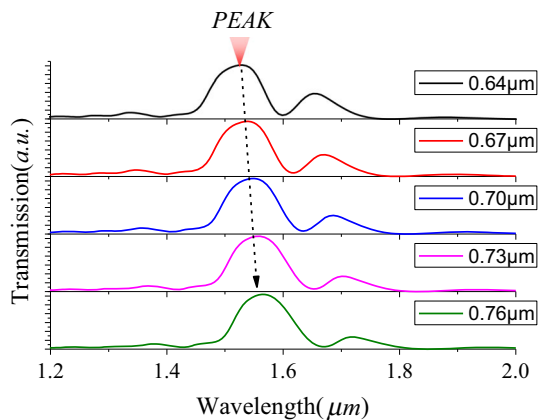


Fig. 6 Transmission spectrum with d from 0.64 to 0.76 μm



proportion of p and d denoted in the two graphs are similar [variations of p and d are shown in expression (3)], we can see clearly that this transmission peak is much more sensitive to p than d . This demonstrates that the resonance mode of the PEAK is a surface plasmon polariton (SPP) mode (Li et al. 2014). Unlike the localized surface plasmon (LSP) mode which is confined to the vicinity of the metal structures, SPP mode is propagating along the dielectric surface (Maier 2007). Because the cavity we designed is based on a small hole to transmit the energy out of the cavity, SPP mode is required for the convergence of energy.

$$\begin{aligned} \text{Variation of } p &: (1.22 \mu\text{m} - 1.02 \mu\text{m}) / 1.12 \mu\text{m} \times 100 \% \approx 17.8 \% \\ \text{Variation of } d &: (0.76 \mu\text{m} - 0.64 \mu\text{m}) / 0.70 \mu\text{m} \times 100 \% \approx 17.1 \% \end{aligned} \tag{3}$$

Figure 7a shows the transmission spectrum of MIM cavity with a variation of incident light polarization angle θ . The inset shows the polarization angle θ along the arrow which is normal to the metal layer. The $|E_z|^2$ distributions at 1.55 μm with θ of 0° and 90° are shown in Fig. 7b, c respectively. When θ is 0° , the light is effectively coupled into the cavity. While with θ of 90° , the incident light is almost blocked outside the cavity, which

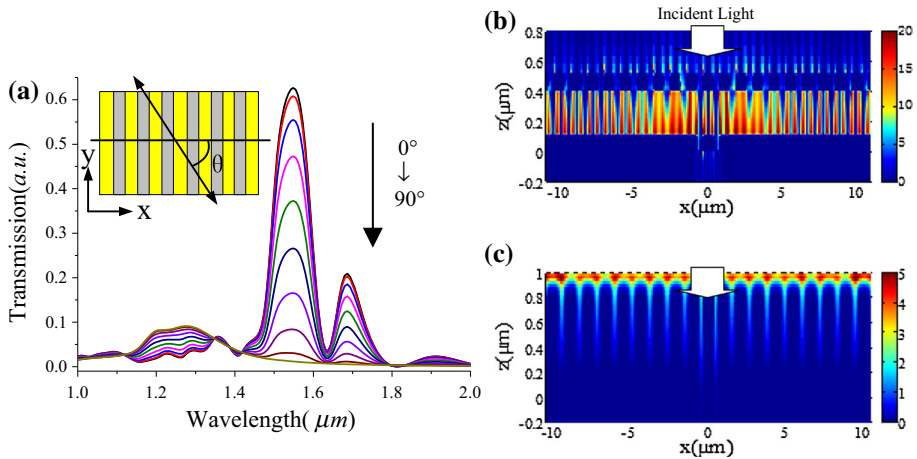


Fig. 7 Polarization selection of the MIM plasmonic focusing cavity. **a** Transmission of MIM cavity with varying the polarization of incident light. **b** $|E_z|^2$ distribution at 1.55 μm with 0° incident polarization angle. **c** $|E_z|^2$ distribution at 1.55 μm with 90° incident polarization angle

makes the peak transmission at 1.55 μm drop almost down to zero as θ increases from 0° to 90°. A polarization ratio of 52 can be realized. The high polarization ratio is very useful for quantum cryptography, which takes polarizations as code modes.

4 Conclusions

A MIM plasmonic focusing cavity is proposed to integrate with the InGaAs/InP APDs. The cavity can effectively couple the light from an incident area as large as 33.6 μm into two sub wavelength holes, with the output light intensity per unit area nine times bigger than that of the input light. The output light travels with little degree of attenuation and a very small divergence angle within only $\pm 0.3^\circ$, which makes it possible to decrease the APD's photo-sensitive diameter to a few micrometers without losing quantum efficiency and suppress the influence of materials defects to the dark count rates and after pulse rates.

Acknowledgments This work was supported by Strategic Pilot Program of Science and Technology of Chinese Academy of Sciences (XDB01010200) and National Natural Science Foundation of China (61405231, 61376053).

References

- Abautret, J., Perez, J.P., Evirgen, A., Martinez, F., Christol, P., Fleury, J., Sik, H., Cluzel, R., Ferron, A., Rothman, J.: Electrical modeling of InSb PiN photodiode for avalanche operation. *J. Appl. Phys.* **113**, 183716 (2013)
- Beveratos, A., Brouri, R., Gacoin, T., Villing, A., Poizat, J., Grangier, P.: Single photon quantum cryptography. *Phys. Rev. Lett.* **89**(18), 187901 (2002)
- Eisaman, M.D., Fan, J., Migdall, A., Polyakov, S.V.: Invited review article: single-photon sources and detectors. *Rev. Sci. Instrum.* **82**(7), 071101 (2011)
- Gedney, S.D.: Introduction to the finite-difference time-domain (FDTD) method for electromagnetics, vol. 1, p. 250. Morgan & Claypool publishers, California (2011)

- Gopal, V., Qiu, W., Hu, W.: Modelling of illuminated current–voltage characteristics to evaluate leakage currents in long wavelength infrared mercury cadmium telluride photovoltaic detectors. *J. Appl. Phys.* **116**, 184503 (2014)
- Hadfield, R.H.: Single-photon detectors for optical quantum information applications. *Nat. Photonics* **3**(12), 696–705 (2009)
- Jiang, X., Itzler, M.A., Ben-Michael, R., Slomkowski, K.: InGaAsP–InP avalanche photodiodes for single photon detection. *IEEE J. Sel. Top. Quantum Electron.* **13**(4), 895–905 (2007)
- Law, S., Podolskiy, V., Wasserman, D.: Towards nano-scale photonics with micro-scale photons: the opportunities and challenges of mid-infrared plasmonics. *Nanophotonics* **2**, 103–130 (2013)
- Li, Qian, Li, ZhiFeng, Li, Ning, Chen, XiaoShuang, Chen, PingPing, Shen, XueChu, Wei, Lu: High-polarization-discriminating infrared detection using a single quantum well sandwiched in plasmonic micro-cavity. *Sci. Rep.* **4**, 6332 (2014)
- Maier, S.A.: *Plasmonics: fundamentals and applications*. Springer Science + Business Media LLC, New York (2007)
- Qiu, W., Hu, W.: Laser beam induced current microscopy and photocurrent mapping for junction characterization of infrared photodetectors. *Sci. China Phys. Mech. Astron.* **58**(2), 027001 (2015)
- Qiu, W., Chen, X.S., Lu, W.: Dark current transport and avalanche mechanism in HgCdTe electron-avalanche photodiodes. *IEEE Trans. Electron Devices* **62**, 1926–1931 (2015)
- Rylander, T., Jin, J.-M.: Perfectly matched layer for the time domain finite element method. *J. Comput. Phys.* **200**(1), 238–250 (2004)
- Stegeman, G.I., Wallis, R.F., Maradudin, A.A.: Excitation of surface polaritons by end-fire coupling. *Opt. Lett.* **8**, 386–388 (1983)
- Sullivan, D.M.: *Electromagnetic simulation using the FDTD method*. Wiley-IEEE Press Series, New Jersey (2000)